All the values of F_c in Table 1 are much lower than the value of 3.8 V/Å that was found in field ion microscope (FIM) experiments for positive Si ions (*17*). Similar reductions of F_c in STM geometry have been seen before (*3, 4, 5*). This effect has been discussed in terms of the overlap of image potentials of tip and sample, which reduces the barrier to field emission (*4, 13*). Recent calculations (*20, 21*) show that, in STM geometry, ions can be emitted at much lower fields than in FIM studies, consistent with the relatively small F_c values determined here.

The F_c values at negative bias are the same, within errors, for all tips, which agrees with the simple picture that F_c is an intrinsic property of the Si, independent of the tip material. There is more scatter at positive bias; but the tip-sample separation is also considerably smaller, so the effects of interaction with the tip may be more pronounced. Although anion emission cannot normally be observed in FIM studies because of the large electron currents generated at negative tip bias (*21*), recent theoretical studies support the view that anion emission should occur at critical fields similar to those for cations (*13, 20, 21*).

The values of A are of the order 1 to 10 $Å^2$ at positive bias but are considerably larger at negative bias. However, it would be overly simplistic to interpret these differences solely in terms of variations of the tunneling area. For example, in more detailed treatments of the tunneling equation at low bias (*22*), other parameters enter into the exponential prefactor, such as the electronic density of states of the emitter. To further investigate such effects, a more detailed theory of tunneling is needed in the medium voltage regime where $V \sim \Phi$. We note that in the fitting procedure, A couples strongly to the values of Φ_t and Φ_s. This is a large source of uncertainty because the quoted values of work functions vary considerably (*19*). The values that we used for the metal tips were based on contact-potential measurements that related to a standard value for W (*19*). For Si, a standard value of 4.8 eV was used (*16*). The errors in Table 1 include a ±0.2 eV variation in the work function values.

We stress the importance of tip preparation in achieving reproducible results. For W tips that were not electron-bombarded, groove formation was not reproducible and often did not occur even at tip biases up to 10 V. A possible explanation is the presence of an oxide layer several nanometers thick on the tips (*23*). The field at the sample may be substantially reduced by the presence of this dielectric film near the end of the tip. Electron bombardment effectively removes the oxide over a large area. We note that Au tips can modify the surface in a reproducible way without electron bombardment, presumably because Au is comparatively inert. Thus, we suggest that the discrepancy between our results and earlier attempts (*2*) to modify Si(111) is attributable to tip preparation. This is a controversial hypothesis that deserves further study because it may be important in other STM nanomodification experiments.

With research based on our results, it has recently been shown that single Si atoms can be removed by a brief pulse near the critical voltage (*24*). Such single-atom modification is a probabilistic event because field emission is a thermally activated process. Modification on the scale of the grooves in Fig. 1 may ultimately be of greater technological significance, though, because it is highly reproducible.

REFERENCES AND NOTES

1. J. A. Stroscio and D. M. Eigler, *Science* **254**, 1319 (1991).
2. R. S. Becker *et al.*, *Nature* **325**, 419 (1987).
3. I.-W. Lyo and P. Avouris, *Science* **253**, 173 (1991).
4. H. J. Mamin, P. H. Guethner, D. Rugar, *Phys. Rev. Lett.* **65**, 2418 (1990).
5. S. E. McBride and G. C. Wetsel, *Appl. Phys. Lett.* **59**, 3056 (1991).
6. J. P. Rabe and S. Buchholz, *ibid.* **58**, 702 (1991).
7. T. Schimmel *et al.*, *ibid.*, p. 1039.
8. I.-W. Lyo, P. Avouris, B. Schubert, R. Hoffmann, *J. Phys. Chem.* **94**, 4400 (1990).
9. J. Boland, *J. Vac. Sci. Technol. B* **9**, 764 (1991).
10. With this STM, the vertical range is determined automatically by a prescan of a small region of the desired scan area. Because the Si(111) surface is very flat, the range is typically limited to about 5 Å. Attempts to image atomic structure inside the grooves were unsuccessful.
11. K. D. Brommer, M. Needels, B. E. Larson, J. D. Joannopolous, *Phys. Rev. Lett.* **68**, 1355 (1992).
12. D. M. Eigler *et al.*, *Nature* **352**, 600 (1991).
13. T. T. Tsong, *Phys. Rev. B* **44**, 13703 (1991).
14. E. A. Dobisz and C. R. K. Marrian, *J. Vac. Sci. Technol. B* **9**, 3024 (1991).
15. R. S. Becker, G. S. Higashi, Y. J. Chabal, A. J. Becker, *Phys. Rev. Lett.* **65**, 1917 (1990).
16. T. T. Tsong, *Atom-Probe and Field Ion Microscopy* (Cambridge Univ. Press, Cambridge, 1990.
17. R. Gomer, *IBM J. Res. Dev.* **30**, 428 (1986).
18. J. G. Simmons, *J. Appl. Phys.* **34**, 1793 (1963).
19. D. E. Gray, Ed. *American Institute of Physics Handbook* (McGraw-Hill New York, ed. 3, 1972).
20. N. D. Lang, *Phys. Rev. B* **45**, 13599 (1992).
21. N. M. Miskovsky, C. M. Wei, T. T. Tsong, *Phys. Rev. Lett.* **69**, 2427 (1992).
22. J. Tersoff and D. Hamann, *Phys. Rev. B* **31**, 805 (1985).
23. J. Garnaes, F. Kragh, K. A. Morch, A. R. Tholen, *J. Vac. Sci. Technol. A* **8**, 441 (1990).
24. H. Uchida, D. H. Huang, F. Grey, M. Aono, unpublished data.

25. We thank H. Rohrer, T. T. Tsong, and R. Synder for discussions and H. Uchida and D. H. Huang for allowing us to refer to their results before publication.

8 June 1992; accepted 13 January 1993

Boundary Layer Profiles in Plasma Chemical Vapor Deposition

David S. Green, Thomas G. Owano, Skip Williams,
David G. Goodwin, Richard N. Zare, Charles H. Kruger*

A nonlinear optical spectroscopy based on degenerate four-wave mixing has made possible direct measurements of species temperature and concentration profiles through the boundary layer of a reactive plasma at atmospheric pressure. Spectra were obtained for CH and C_2 radicals over a range of conditions including those for the plasma chemical vapor deposition of diamond films. Numerical simulations based on a one-dimensional stagnation-point flow model are in good agreement with the measurements. The CH mole fraction is shown to rise and fall as a function of distance from the substrate, which is compelling experimental evidence for the complex chemistry that is occurring in the plasma boundary layer.

Plasmas find a wide range of applications from light sources to materials synthesis and even the development of controlled fusion. Yet the contribution of plasmas to emerging technologies relies on our ability to characterize what is among the harshest of chemical environments. The intense luminosity along with the rapidly changing chemistry, temperature, pressure, and velocity challenge our ability to make meaningful measurements and to model such systems. Diagnostics are required to provide information about neutral and ionized species, electron density, and energy in the plasma. Furthermore, the implementation of such diagnostics must be nonintrusive, species- and state-selective, sensitive, and capable of high spatial and temporal resolution. We report the use of resonant degenerate four-wave mixing (DFWM) (*1, 2*) to probe the boundary layer chemistry of an atmospheric-pressure radio-frequency, inductively coupled plasma. As a representative system, we used an industrial-scale reactor and made in situ measurements of the temperature and concentration of CH

D. S. Green, S. Williams, R. N. Zare, Department of Chemistry, Stanford University, Stanford, CA 94305.
T. G. Owano and C. H. Kruger, High Temperature Gasdynamics Laboratory, Department of Mechanical Engineering, Stanford University, Stanford, CA 94305.
D. G. Goodwin, Division of Engineering and Applied Science, California Institute of Technology, Pasadena, CA 91125.

*To whom correspondence should be addressed.

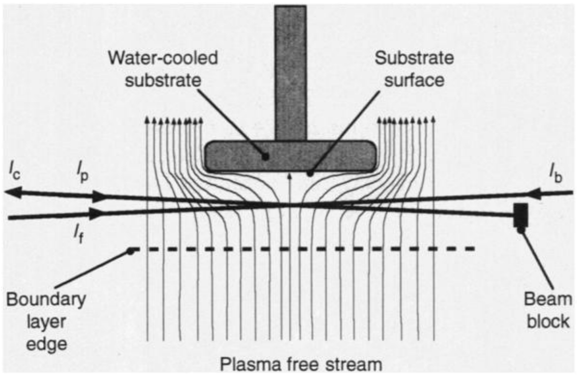

Fig. 1. Schematic of the stagnation-point flow geometry showing the boundary layer (not to scale). The two counterpropagating and collinear pump beams are indicated as forward and backward beams (I_f and I_b). The probe beam is designated I_p, and the conjugate beam is the DFWM signal beam I_c.

and C_2 radicals under conditions that include those used for the plasma chemical vapor deposition (PCVD) of diamond films (*3, 4*). We observed that under certain conditions the CH concentration rises and falls in the boundary layer, in close agreement with numerical simulations.

One of the distinctive features of atmospheric-pressure PCVD, in contrast to low-pressure environments, is the presence of a thin (<1 cm) boundary layer near the surface. As the hot plasma impinges on the colder surface, the flow is diverted; this results in a boundary layer characterized by chemical nonequilibrium and steep gradients in velocity, temperature, and composition. This layer is important chemically because it defines a restricted reaction zone for the production and destruction of molecular species. In Fig. 1 we show schematically the stagnation flow geometry and the intersecting laser beams that are used to probe selected volumes within the boundary layer. The radicals present in the bulk plasma may diffuse through the boundary layer and will have varying rates for recombination or reaction in the gas phase and at the surface. But the growth of a complicated material, such as diamond, is a complex mechanistic process that involves many reaction intermediates. Critical to the deposition process are the energized transient radicals created in the boundary layer. Therefore, to understand the chemical mechanisms that govern PCVD as well as the fundamentals of plasma chemistry, it is necessary to investigate the coupled effects of convection, diffusive transport, gas-phase chemistry, and gas-surface chemistry.

The use of DFWM as an optical diagnostic of plasmas is a promising alternative to many conventional laser-based spectroscopies that are intractable in these harsh environments (*1*). This spectroscopy is very sensitive and has been used successfully to monitor atomic (*5–8*) and molecular (*9–13*) species for combustion diagnostics as well as atoms in a low-pressure discharge (*14*). The DFWM signal is a spatially coherent, polarized beam that can be collected with high efficiency and filtered against background interferences from incoherent light (*1*). The ability to use this technique to detect species at levels approaching 10^{10} molecules per cubic centimeter in flames and discharges has obvious advantages for tracking transient and highly reactive chemical intermediates. In addition, DFWM in the phase-conjugate configuration is a sub-Doppler spectroscopy that is superior to linear techniques in selectivity and state specificity. Furthermore, spatial resolution on the scale of micrometers can be obtained with sample volumes defined by the overlap of the three incident beams.

To quantify the DFWM process, the two-level model proposed by Abrams *et al.* (*2*) is usually applicable (*1, 5–14*). If we assume low optical density and conditions of saturation, the DFWM signal intensity is directly proportional to the square of the population difference ΔN^2. The DFWM signals are sensitive to laser intensity, absorber motion, pressure, and level-dependent processes. Although "real" systems are complicated, DFWM determinations of absolute concentrations should be possible and certainly relative concentrations can be obtained. Temperature measurements can be made by fitting the intensities from well-resolved rovibrational lines to a Boltzmann distribution (*10, 13*).

The experimental setup for our DFWM experiment is known as the phase conjugate geometry (*1, 2*). The laser source is a conventional neodymium:yttrium-aluminum-garnet pumped dye laser system that provides 5-ns pulses of 0.05-cm^{-1} bandwidth. The light is spatially filtered and passed through a series of beam splitters that yield three input beams of equal intensity. The maximum energy of the beams is maintained near 10 μJ per pulse (yielding intensities in excess of saturation). Both the forward pump beam I_f and the probe beam I_p are vertically polarized, while the backward pump beam I_b is horizontally polarized. With the forward pump and probe at an angle of 2.5°, the interaction volume is defined by a path length of approximately 1 cm and beam waists of less than 500 μm. The conjugate beam I_c, the DFWM signal, is extracted from the probe beam path with a 1:1 beam splitter, passed through a linear polarizer and spatial filter, and collected by a photomultiplier tube ~8 m away from the luminous plasma.

Diagnostics of plasma chemistry require not only well-designed experiments but also theoretical models. The difficulties in developing these models lie in the inherent complexity of high-temperature gas-phase and gas-surface chemistry and the lack of necessary kinetic and thermophysical data. In our studies, we draw on a computational simulation developed for diamond PCVD (*15*). The robustness of the model can be judged by its successful application to many deposition systems, including hot filaments, arc jets, flames, and rf plasma torches (*4, 15, 16*). This is a one-dimensional stagnation-point flow model that includes coupled gas-phase chemistry, multicomponent diffusion including thermal diffusion, and surface chemistry. The gas-phase chemical reaction mechanism consists of 50 reactions. The diamond growth mechanism is a modified form of the methyl-based mechanism proposed by Harris (*17*). The model is used to predict gas-phase temperature and velocity profiles, concentration profiles for 20 chemical species (Ar, H, H_2, all C_1- and

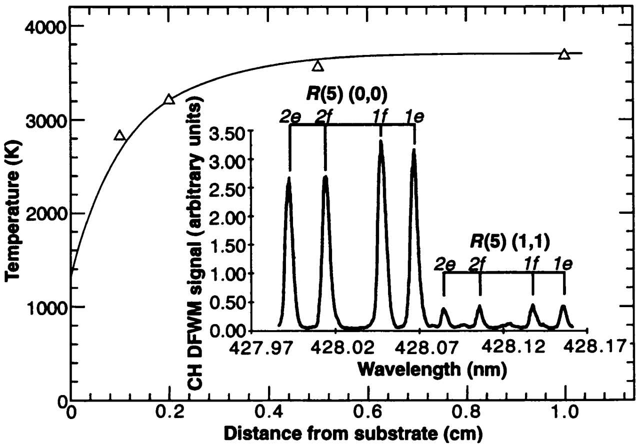

Fig. 2. The CH temperature profile determined from DFWM measurements (△) and that calculated (—) from numerical simulation, where $T_{\text{free stream}} \approx 3700$ K and $T_{\text{substrate}} \approx 1300$ K. (**Inset**) Representative DFWM spectrum of the CH $A^2\Delta$–$X^2\Pi$ (0,0) and (1,1) band systems in the region of the *R*(5) rotational lines, at $T_{\text{vib}} \approx 3700$ K.

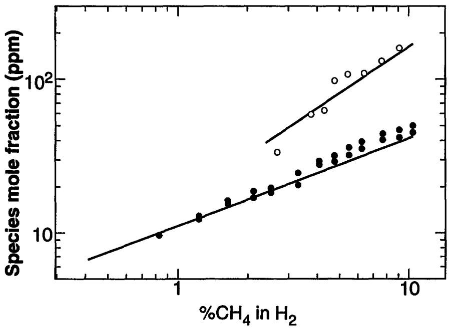

Fig. 3. Results of a stoichiometric study that compares DFWM measurements of the relative CH (●) and C_2 (○) mole fractions in the free stream with an equilibrium calculation (—) at $T_{\text{free stream}}$ = 3500 K as a function of CH_4 feed-gas flow. The Ar and H_2 flows are fixed at 106.5 and 12 liter min^{-1}, respectively.

C_2-hydrocarbons, as well as several C_3- and C_4-hydrocarbons), and deposition rates as a function of temperature, gas mixture, and total pressure. In the past, this model has been used as a sensitive test of growth rates (*4, 15*). In contrast, this work examines the model's predictive ability to trace the chemistry of reactive gas-phase intermediates at higher temperatures, under collision-dominated atmospheric-pressure conditions.

The chemistry encountered during atmospheric-pressure plasma synthesis of diamond thin films consists of the nonequilibrium reactions that occur within the boundary layer. The species of interest include atomic hydrogen, which participates in such processes as activation of surface sites and extraction during hydrocarbon addition. The carbon is drawn from a variety of species such as C_1H_m (m = 0 to 4) and C_2H_n (n = 0 to 6). It is the nonequilibrium processes between hydrogen and the radicals near the surface that enhance diamond growth kinetics under temperature and pressure conditions that would otherwise make diamond deposition impossible.

The high spectral, spatial, and temporal sensitivity of DFWM allows us to measure the spectra of CH and C_2 as a function of position in the boundary layer and to derive local temperature profiles. We select the rotational lines of the CH $A^2\Delta$–$X^2\Pi$ (0,0) and (1,1) band systems near 431 nm and the C_2 $d^3\Pi_g$–$a^3\Pi_u$ (2,0), (3,1), and (4,2) band systems near 437 nm for study. The spectral region displayed in Fig. 2 shows the $R(5)$ rotational lines of CH. All fine structure and Λ-doublet components of CH are clearly resolved. Also shown in Fig. 2 is a comparison between the CH vibrational temperature determined by DFWM measurements at various distances from the substrate and the profile predicted by the one-dimensional flow model. Here we apply the relation $I_c \propto N^2$ and evaluate the temperature using relative DFWM signal intensities from corresponding rotational components and the ratio of Boltzmann factors. The simulated profile is calculated by adopting the DFWM-measured free-stream vibrational temperature of 3700 K and the pyrometrically measured surface temperature of 1300 K as boundary conditions. Good agreement is found between the numerical simulation and DFWM measurements.

Stoichiometric studies use DFWM diagnostics to monitor the relative change in the mole fraction of CH and C_2 as a function of the CH_4 feed-gas flow at fixed temperature and Ar:H_2 mixing ratio. Such investigations are motivated by previous work (*4*) in which it was reported that there is a narrow parameter range in which diamond films are grown and in which it was shown that gas-feed ratios have a dramatic effect on growth rates. Figure 3 illustrates the result of stoichiometric measurements in the free stream. The DFWM data reflect a simple N^2 signal dependence, and we evaluated the Boltzmann factors using an experimentally derived temperature of 3500 K. The calculated equilibrium concentrations and the DFWM measurements show excellent agreement. Consequently, the stoichiometric studies confirm that relative species concentrations determined by DFWM measurement are consistent with equilibrium chemistry in the free stream.

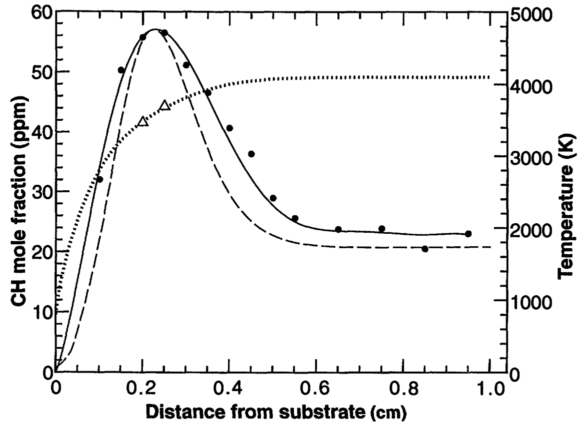

Fig. 4. Comparison between the CH concentration profile determined from DFWM measurements (●) [with a spline curve (—) fit to the data points] and that calculated (----) from numerical simulation, where $T_{\text{free stream}} \approx$ 4100 K and $T_{\text{substrate}} \approx$ 800 K. Also shown are vibrational temperature measurements (△) and the simulated temperature profile (····).

A comparison of the predicted CH temperature and mole fraction profiles based on the one-dimensional stagnation-point flow model with the DFWM measured temperature and relative mole fraction profiles is shown in Fig. 4. We used harsher plasma conditions here than in the above experiments to obtain steeper temperature gradients and to test the ability of DFWM diagnostics to track the rise and fall of radical concentrations in the boundary layer. On the basis of integrated signal intensity ratios between rotational components of the CH (0,0) and (1,1) bands, we evaluated the vibrational temperature at a number of positions close to the maximum of the concentration profile. We found that these temperature measurements, in conjunction with a surface temperature determined by optical pyrometry, are sufficient to define thermal boundary conditions for the numerical simulation (yielding a free-stream temperature of 4100 K). Additional boundary conditions adopted in this simulation are a free-stream velocity of 10 m s^{-1} and a surface temperature of 800 K. The predicted thermal boundary layer is about 5 mm thick and falls steeply close to the surface. We have found good agreement between numerical simulations and DFWM measurements of vibrational temperature from 2000 to 4500 K. The drop in strength of the CH (1,1) bands in the cooler regions hinders the evaluation of vibrational temperatures for distances smaller than 1 mm above the surface. Yet we are encouraged by the fact that the rotational structure of the CH (0,0) band spectrum remains strong even close to the surface and should provide rotational temperature profiles to within 100 μm.

The mole fraction profiles in Fig. 4 illustrate the sensitivity of DFWM diagnostics to the production and destruction of CH concentration within the boundary layer for a characteristic set of plasma conditions. The relation $I_c \propto N^2$ is considered valid, and we normalize the relative DFWM measurements to the peak predicted value. The Boltzmann factors are obtained from the simulated thermal profile defined by the gas-phase and surface temperature measurements. The CH mole fraction goes through a maximum inside the thermal boundary layer at a distance of about 2.5 mm from the surface, while in the same region the temperature decreases monotonically (Fig. 4). These results show excellent agreement between the DFWM-measured relative species profile and the numerical simulation.

Such measurements when compared with theoretical models provide valuable information on the role of partial equilibrium among the C_1- and C_2-species with atomic hydrogen. The correct prediction of the temperature and concentration profiles are a vital test of our ability to understand plasma chemistry at the boundary layer, specifically the dependence on gas-phase reactions and the contribution of surface reactions.

REFERENCES AND NOTES

1. R. L. Farrow and D. J. Rakestraw, *Science* **257**, 1894 (1992).
2. R. L. Abrams, J. F. Lam, R. C. Lind, D. G. Steel, P. F. Liao, in *Optical Phase Conjugation*, R. A. Fisher, Ed. (Academic Press, New York, 1983), p. 211.
3. The plasma is produced by a commercial, atmospheric-pressure radio frequency, inductively coupled, plasma torch. Typical feed-gas conditions (in liters per minute) are: Ar, 106.5; H_2, 12.0; and CH_4, 0.55. The net plasma enthalpy is about 7 kW leaving the nozzle exit, and the free-stream electron density is on the order of 10^{15} cm^{-3}. Substrates are held by a translation stage and positioned in the stagnation flow geometry of Fig. 1. A molybdenum substrate with surface temperature maintained near 1300 K is used for plasma conditions that promote diamond deposition. When the plasma is driven to higher temperatures and beyond diamond synthesis conditions, a water-cooled copper disk is substituted for the molybdenum substrate.
4. T. G. Owano, C. H. Kruger, M. A. Cappelli, *Mater. Res. Soc. Symp. Proc.* **190**, 131 (1991); M. A. Cappelli, T. G. Owano, C. H. Kruger, *J. Mater. Res.* **5**, 2326 (1990); T. G. Owano, C. H. Kruger, D. G. Goodwin, in preparation.
5. J. Pender and L. Hesslink, *Opt. Lett.* **10**, 264 (1985).
6. J. M. Ramsey and W. B. Whitten, *Anal. Chem.* **59**, 167 (1987).
7. P. Ewart, P. Snowdon, I. Magnusson, *Opt. Lett.* **14**, 563 (1989).
8. W. G. Tong, J. M. Andrews, Z. Wu, *Anal. Chem.* **59**, 896 (1987); J. M. Andrews and W. G. Tong, *Spectrochim. Acta Part B* **44**, 101 (1989); J. M. Andrews, K. M. Weed, W. G. Tong, *Appl. Spectrosc.* **45**, 697 (1991).
9. P. Ewart and S. V. O'Leary, *Opt. Lett.* **11**, 279 (1986); P. Ewart and M. Kaczmarek, *Appl. Opt.* **30**, 3996 (1991).
10. T. Dreier and D. J. Rakestraw, *Opt. Lett.* **15**, 72 (1990); *Appl. Phys. B* **50**, 479 (1990); D. J. Rakestraw, R. L. Farrow, T. Dreier, *Opt. Lett.* **15**, 709 (1990).
11. B. Yip, P. M. Danehy, R. K. Hanson, *Opt. Lett.* **17**, 751 (1992).
12. B. A. Mann, S. V. O'Leary, A. G. Astill, D. A. Greenhalgh, *Appl. Phys. B* **54**, 271 (1992).
13. S. Williams, D. S. Green, S. Sethuraman, R. N. Zare, *J. Am. Chem. Soc.* **114**, 9122 (1992).
14. D. A. Chen and W. G. Tong, *J. Anal. At. Spectrom.* **3**, 531 (1988); W. G. Tong and D. A. Chen, *Appl. Spectrosc.* **41**, 586 (1987).
15. D. G. Goodwin, *Appl. Phys. Lett.* **59**, 277 (1991); ______ and G. G. Gavillet, *J. Appl. Phys.* **68**, 6393 (1990).
16. S. J. Harris and D. G. Goodwin, *J. Phys. Chem.* **97**, 23 (1993).
17. S. J. Harris, *Appl. Phys. Lett.* **56**, 2298 (1990).

18. D.S.G. is a Natural Science and Engineering Research Council (Canada) postdoctoral fellow. S.W. is an Air Force Office of Scientific Research graduate scholar. This work was supported by several sources: C.H.K. acknowledges support from the Department of Energy under contract DE-FG03-88ER13957 and R.N.Z. from the Department of Energy under contract DE-FG03-92ER14304.

26 October 1992; accepted 23 December 1992

Cryptic Grain-Scale Heterogeneity of Oxygen Isotope Ratios in Metamorphic Magnetite

John W. Valley* and Colin M. Graham

Oxygen isotope ratios measured by ion microprobe in magnetite from granulite-facies marble of the Adirondack Mountains, New York, range from +2 to +11 per mil (standard mean ocean water) across a single grain that measures 3 millimeters by 5 millimeters. Low values are concentrated in irregular domains near the grain boundary but also occur in the grain's interior. In contrast, grains 1 millimeter in diameter that are from a second nearby sample show no significant heterogeneity, except within 10 micrometers of the grain boundary. These data, including large gradients of up to 9 per mil per 10 micrometers, provide important new constraints on the nature and origins of intragrain isotopic heterogeneity and on oxygen isotope thermometry. The differences between these magnetite grains result from contrasting mechanisms of isotope exchange with fluids after the peak of regional metamorphism. Volume diffusion of oxygen through the crystal structure of magnetite contributed to isotope exchange in the rims of small grains, but larger grains are crosscut by healed cracks that are not readily detected and that short-circuited diffusion.

The fractionation of oxygen isotopes between coexisting minerals should, in theory, provide an ideal means by which to determine the temperature of formation for many rocks (*1–5*). Appropriate mineral assemblages are plentiful, fractionation coefficients are well calibrated, temperature sensitivity is good, and there is no measurable pressure correction. However, the actual reliability of the results of stable isotope thermometry in igneous and metamorphic rocks is controversial (*1, 4, 6–11*).

Thermometers have often been thought to reset after mineral crystallization by exchange within and among minerals. Experimental data on oxygen self-diffusion in minerals have been used in models of retrograde exchange and, in some cases, in estimates of cooling rates (*7–10, 12*). The approximate agreement of two or more temperatures estimated from different mineral pairs in the same rock is often taken as proof that the estimate is accurate, but apparent agreement can arise in spite of retrogression.

Recent numerical modeling has shown that, because grain boundaries are zones of relatively rapid diffusion, there is not a simple blocking-temperature relation for diffusion [as in (*13*)]. In addition, closed-system exchange depends on modal proportions of all of the minerals in a rock as well as their mineral diffusivities, grain sizes, grain shapes, and cooling rates (*10*). Furthermore, oxygen diffusivity in some minerals is greatly enhanced by high water or proton activity (*14, 15*). In the presence of fluids, oxygen exchange may also occur by solution reprecipitation or reaction rather than by diffusion (*8, 11, 14, 16, 17*). Thus, the removal of grain boundary fluid by retrograde reactions during the cooling of a metamorphic rock could cause sudden cessation of oxygen diffusion. These observations raise the possibility that individual mineral grains might preserve microscale information of their thermal or fluid-rock interaction histories (*7*).

Advances in the microanalysis of stable isotope ratios in minerals by the ion microprobe–secondary ion mass spectrometer have allowed researchers to decipher the isotopic record within individual mineral grains as initially demonstrated for magnetite (*7*). In well-constrained cases where zonation patterns are known, their interpretation can provide a more fundamental understanding of the thermal evolution and the fluid-rock interaction in the Earth's crust.

In this report, we describe the first detailed mapping of oxygen isotope ratios in a single mineral grain, a large magnetite crystal from a granulite facies marble from the Adirondack Highlands, New York, and discuss implications for the processes that redistribute oxygen during cooling of metamorphic rocks. The magnetite crystal is from the Weston Mine, a magnetite skarn at the contact of the Marcy anorthosite massif in the central Adirondack Highlands. These rocks have experienced a complex metamorphic history (*18, 19*) of contact metamorphism and metasomatism (~900°C, <3 kbar), regional Grenville-age (1080 to 1050 million years ago) granulite facies metamorphism at about 775°C and 7.5 kbar, and finally late-stage alteration during slow cooling, 1° to 3°C per million years (*20*). Large amounts of aqueous fluids were involved during skarn formation, small amounts of grain boundary fluids were present during

---

J. W. Valley, Department of Geology and Geophysics, University of Wisconsin, Madison, WI 53706.
C. M. Graham, Department of Geology and Geophysics, University of Edinburgh, Edinburgh EH9 3JW, Scotland, United Kingdom.

---

*To whom correspondence should be addressed.